Technical Analysis of Hydrogen Production System Using Concentrated Photovoltaic Thermal/Organic Rankine Cycle (CPVT/ORC) System

MOHAMMAD HOSEIN JAHANGIR[1,*], RAHIM MOLTAMES [1], REZA FATTAHI [1,2], AND HOSSEIN YOUSEFI[1]

[1] *Faculty of New Sciences and Technologies, university of Tehran, Tehran, Iran*
[2] *Renewable Energy and Energy Efficiency Organization (SATBA), Tehran, Iran,*
[*] *Corresponding author email: mh.jahangir@ut.ac.ir*

Manuscript received 01 February, 2023; revised 08 July, 2023; accepted 28 August, 2023. Paper no. JEMT-2302-1430.

There is growing concern about the release of pollutants from the use of fossil fuels. These concerns have led to the increased use of renewable energy sources and green energy carriers such as hydrogen. This paper evaluates a new hydrogen production system using a solar energy source. For this purpose, the concentrated photovoltaic (CPV) system is used for the first time as the driver of the proposed hydrogen production system. The first and second laws of thermodynamics and the conservation of mass and energy are used to simulate the system. The results show that the PV production power is 1529.4 kW, the turbine output power is 1015.3 kW, the pump consumption power is 126.5 kW, the hydrogen production is 6 grams per second, the energy efficiency is 8.84% and the exergy efficiency is 36.77%. On the other hand, the parametric analysis shows that increasing the nominal efficiency of the PV panel increases the PV power generation, in addition, increasing the ambient temperature decreases the PV power generation. Also, increasing the fluid quality at the evaporator outlet increases the energy efficiency and exergy.

keywords: *Electricity Consumption, Spatiotemporal Monitoring, Statistical Process Control, Residual-based Control Chart, Autocorrelation.*

http://dx.doi.org/10.22109/JEMT.2023.384215.1430

1. INTRODUCTION

Hydrogen plays a key role in the transition to sustainable societies. Hydrogen will have wide applications in various industries, including land and air transportation, feed chemical industries, and energy carriers in storage and production systems [1]. However, about 95% of the consumed hydrogen is produced by hydrocarbon steam reforming, which is responsible for emitting 830 million tons of carbon dioxide per year worldwide [1]. Obviously, this situation is not very suitable. Hydrogen production should be produced with more modern technologies and using renewable energy sources.

The use of renewable energy sources for hydrogen production purposes reduces carbon emissions and promotes sustainability. However, further research and development are needed to optimize this technology and make it commercially viable on a large scale. Overall, the coupling of solar power system and electrolyzer represents a promising avenue for advancing the production of hydrogen as an energy carrier. Solar energy has the highest capacity among other energy sources [2]. The performance of a PEM electrolyzer system was analyzed by Awasthi et al. [3] through the development of a computational model that examined the impact of different operating conditions and electrolyzer components. Ganjehsarabi et al. [4] assessed the performance of a solar-driven high-pressure PEM electrolyzer. They used the variable solar irradiance data sets to analyze the performance of the proposed system. Their results showed that the inverter size should be larger than 0.75% of maximum excess power to have a higher efficiency. Burton et al. [5] reviewed the methods of hydrogen production efficiency increment. They revealed that further advances in the efficient production of renewable hydrogen will require the consideration of the molecular dynamics of the water molecule. Nafchi et al. [6] investigated the performance of a solar-based hydrogen and electric power generation plant incorporated with a high-temperature PEM electrolyzer and energy storage. Their results showed that integration of the PEM electrolyzer enhances the exergy efficiency of

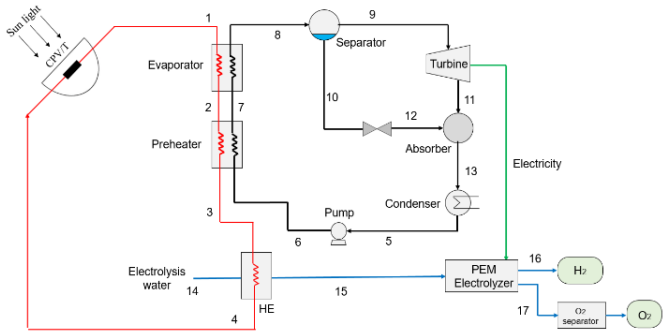

Fig. 1. Schematic of the studied system

the Rankine cycle, considerably. However, it causes almost 5% exergy destruction in the integrated system due to conversion of electrical energy to hydrogen energy. Also, they concluded that increase of working pressure and membrane thickness leads to higher cell voltage and lower electrolyzer efficiency. Their results indicated that the integrated system is a promising technology to enhance the performance of concentrating solar power plants. M. Alirahmi et al. [7] developed a multi-criteria optimization model for optimizing the solar thermal power plant integrated with a PEM electrolyzer and thermoelectric generator. They used the Genetic Algorithm (GA) for searching optimal results of their proposed system. Their results showed that the specific cost of the system product and the exergy efficiency is 30.2$/GJ and 21.9%, respectively, and the produced hydrogen rate is 2.906 kg/h. O. Rejeb et al. [8] proposed a solar-driven poly-generation system for Oxygen, Hydrogen, Electricity, and Heat production. They considered energy efficiency, cost rate, and net output power as the objective function of the optimization model. The results show that the proposed system operates with an exergy efficiency of 16.24%, a cost rate of 4.48 $/hr, and a net electrical power of 33.32 kW under optimal conditions.

In addition, some researchers have evaluated the technical and economic aspects of the proposed concentrated photovoltaic integrated with an organic Rankine cycle for electricity production purposes [9–12]. They used the zero-dimensional energy model to evaluate the thermal behavior of system layers in order to determine the heat losses, and consequently, the energy output.

Despite the extensive studies in this field, no study has been carried out to evaluate the concentrated photovoltaic system for the proposed hydrogen production system. In this article, we have designed a system in which not only the power generated by the PV is used directly to produce hydrogen, but also its recycled heat is converted into electricity using the Organic Rankine Cycle and used again to produce hydrogen by the electrolyzer

2. METHODOLOGY

In this project, an organic Rankin cycle with a geothermal input energy source is used to supply the electric power required for hydrogen production. The schematic of the system studied in this paper is shown in Figure 1. In the proposed system, the solar energy is used as the input energy of thermal system. The working fluid at the outlet of the condenser is in a saturated liquid state (point 5). The pump raises the fluid pressure and directs it to the pre-heater (point 6). In the evaporator, the liquid is vaporized through heat transfer from the geothermal water to the working fluid of the organic Rankine cycle and then enters the phase separator (point 8). The separator directs the saturated vapor phase to the turbine inlet (point 9) and directs the liquid phase to the pressure breaker (point 10). The entering steam to turbine causes the turbine to rotate and exits with low pressure (point 11), which finally mixes with the fluid exiting the pressure breaker in the absorber (point 13). Finally, the liquid is condensed in the condenser and the organic Rankine cycle is completed. The work output of the turbine is converted into electrical energy in the generator and finally the electrical energy enters the Electrolyzer to produce hydrogen. Each of the subsystems is described below.

A. Photovoltaic system

The concentrated photovoltaic system used in the simulation consists of a linear parabolic concentrator and a photovoltaic panel at its center. It should be noted that the dimensions used in this article for the design of the system are small-scale, and its results can be generalized to large-scale designs. The area of the panel used in the system is 1 square meter, where the panel length is 10 times its width. The area of the concentrator is obtained according to the dimensions of the panel and the concentrator's collection coefficient.

$$A_{con} = C \times A_{pv} \quad \textbf{(1)}$$

where A_con is the concentrator area (m^3), C is the concentration ratio, and A_pv is the PV panel area (m^2).

At the beginning of system design, the concentrator collection coefficient is considered a fixed initial value. This value will be changed after the full introduction of the system and during the sensitivity analysis that will be done for this coefficient. In the analysis of the photovoltaic system, solar radiation equal to 1000 W/m^2, ambient temperature 25°C and wind speed 2 m/s are considered. Photovoltaic panel efficiency according to its working temperature is obtained by the following relation [13]:

$$n_{pv} = n_{pv-ref}[1 - \beta_{ref}(T_{pv} - T_{ref})] \quad \textbf{(2)}$$

where n_pv is the PV panel efficiency (%), $n_(pv - ref)$ is the PV nominal efficiency (%), β_{ref} is the temperature coefficient (1/K), T_pv is the PV panel temperature (K), and T_ref is the reference temperature (298.16K).

In order to calculate the output power of the panel, it is necessary to calculate the radiant power falling on the panel by the concentrator. Radiant power landing on the panel (Qpv) is calculated according to the following equation:

$$Q_{pv} = GCn_{optical}A_{pv} \quad \textbf{(3)}$$

The output power of the panel (Ppv) is obtained according to the following equation according to the radiant power falling on it:

$$P_{pv} = Q_{pv}n_{pv}n_{inv} \quad \textbf{(4)}$$

Radiant power falling into the system is partially converted into electrical power according to equation 5 and the rest is converted into thermal power, whose amount can be calculated according to the following equation:

$$Q_{Th} = Q_{pv}(1 - n_{pv}) \quad \textbf{(5)}$$

From this thermal power produced in the system, a part is lost by radiation caused by the higher temperature of the system than the environment and convective heat transfer, and a part is

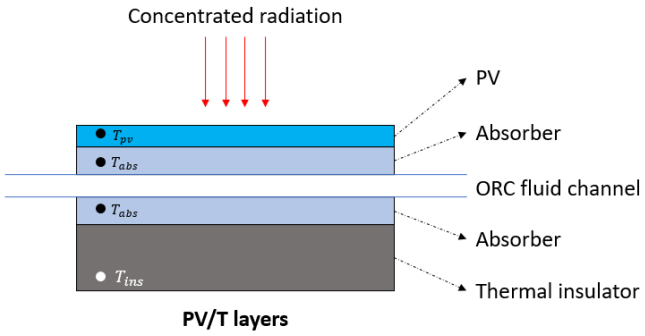

Fig. 2. Layers used in the photovoltaic-thermal system

delivered to the organic Rankin cycle, which is written according to equation 6:

$$Q_{Th} = Q_{orc} + Q_{rad} + Q_{conv} \quad (6)$$

The convective and radiant thermal power resulting from the higher temperature of the photovoltaic system compared to its environment are written as follows, respectively:

$$Q_{conv} = h_{pv}A_{pv}(T_{pv} - T_a) + h_{ins}A_{pv}(T_{ins} - T_a) \quad (7)$$

$$Q_{rad} = \varepsilon_{pv}A_{pv}\sigma(T_{pv}^4 - T_a^4) + \varepsilon_{ins}A_{pv}\sigma(T_{ins}^4 - T_a^4) \quad (8)$$

To obtain the temperature of different layers used in the system (Figure 2), it is necessary to use an energy balance model along the system. Due to the thickness of the layers, the temperature is almost constant throughout each of the layers, therefore, the zero-dimensional energy balance model can be used for simulation (Figure 2). The energy balance around each layer used in CPVT system is as follows [14]:

The energy balance around photovoltaic panels:

$$\begin{aligned} &m_{pv}C_{p,pv}\frac{dT_{pv}}{dt} = h_{pv}A_{pv}(T_a - T_{pv}) \\ &+\varepsilon_{pv}A_{pv}\sigma(T_a^4 - T_{pv}^4) \\ &+A_{pv}\left(\frac{T_{abs}-T_{pv}}{R_{pv-abs}}\right) + Q_T \end{aligned} \quad (9)$$

The energy balance around the absorber plate:

$$\begin{aligned} &m_{abs}C_{p,abs}\frac{dT_{abs}}{dt} = A_{pv}\left(\frac{T_{pv}-T_{abs}}{R_{pv-abs}}\right) \\ &+A_{pv}\left(\frac{T_{ins}-T_{abs}}{R_{abs-ins}}\right) - Q_{orc} \end{aligned} \quad (10)$$

The energy balance around the insulation board:

$$\begin{aligned} &m_{ins}C_{p,ins}\frac{dT_{ins}}{dt} = A_{pv}\left(\frac{T_{abs}-T_{ins}}{R_{abs-ins}}\right) \\ &+h_{ins}A_{pv}(T_a - T_{ins}) \\ &+\varepsilon_{ins}A_{pv}\sigma(T_{sky}^4 - T_{ins}^4) \end{aligned} \quad (11)$$

The temperature of the sky calculated according to the following equation [15]:

$$T_{sky} = 0.0552T_a^{1.5} \quad (12)$$

The energy balance around the coolant:

$$m_{fl}C_{p,fl}\frac{dT_{fl}}{dt} = \dot{m}_{r245fa}(h_{in} - h_{out}) + Q_{orc} \quad (13)$$

At the point of design and by ignoring the transient state, the temperature of each component used in the system can be considered constant during one hour. Therefore, the left-hand side of the energy balance equations around the layers will be zero. The coefficient of heat transfer (h) is considered the same for both sides of the module [13] and is expressed by the following relationship (heat transfer from the edges is ignored):

$$h = 2.8 + 3V_{wind} \quad (14)$$

The temperature of the photovoltaic panel will be about 10 °C higher than the temperature of the cooling fluid output [16]. Repetitive and simultaneous solving of the above equations leads to the calculation of the values of variable parameters such as the temperature of different layers in the photovoltaic panel and finally the energy input to the organic Rankin cycle.

B. PEM Electrolyzer

Polymer Electrolyte Membrane (PEM) electrolyzers are one of the most common energy converters to produce hydrogen. An electrolyzer consists of several electrolyzer cells that are connected in series. In an electrolyzer, water is produced by passing an electric current through two electrodes separated by an electrolyte. It breaks down into hydrogen and oxygen. According to Faraday's law, the rate of hydrogen production in an electrolyzer cell is directly proportional to the transfer rate of electrons in the electrodes, which is actually equal to the electric current in the circuit. The main components of electrolyzers are cathode, anode, electrolyte, and separator. Based on the type of these components, electrolyzers are divided into five main categories: traditional and advanced alkaline electrolyzers, PEM electrolyzers, inorganic membrane electrolyzers and solid oxide electrolyzers. Currently, the alkaline electrolyzer, whose electrolyte is liquid, and the PEM electrolyzer, whose electrolyte is solid, are the most common electrolyzers. Between these two, the alkaline electrolyzer is older and is suitable for medium to high-end devices. The PEM electrolyzer is mostly used for small scale. Among the types of electrolyzers, PEM electrolyzers have many relative advantages, including higher voltage efficiency, performance, and efficiency, higher current density (up to 13 ampere per square meter), production of pure hydrogen and oxygen, greater safety (no circulation of corrosive electrolyte), compact And being small in size, significantly increasing the efficiency in case of increasing the working temperature up to 450°C and faster response to variable electrical inputs are more useful. Among the disadvantages of PEM electrolyzers, we can mention the high cost of the components and the corrosive acidic environment. Hence, in this research, the PEM electrolyzer has been studied. Figure 3 shows the schematic of the PEM electrolyzer. The reactions in the anode and cathode of a PEM electrolyzer are written as follows [17]:

$$Anode: H_2O \rightarrow 2H^+ + \frac{1}{2}O_2 + 2e^- \quad (15)$$

$$Cathode: 2H^+ + 2e^- \rightarrow H_2 \quad (16)$$

$General Reaction: H_2O_{(L)} \rightarrow H_{2(g)} + \frac{1}{2}O_{2(g)}$ Based on the Gibbs free energy of reaction, there is a reversible voltage for PEM electrolyzer. This voltage corresponds to the ideal electrolyzer cell in reversible and isothermal conditions. In fuel cells, all the electrical energy obtained during the process of electron movement is available in an external circuit. The concept for the electrolyzer is that all the kinetic energy produced is available for hydrogen production without any loss, the rest of the voltage drops are added to the reversible voltage and corrected to account for the

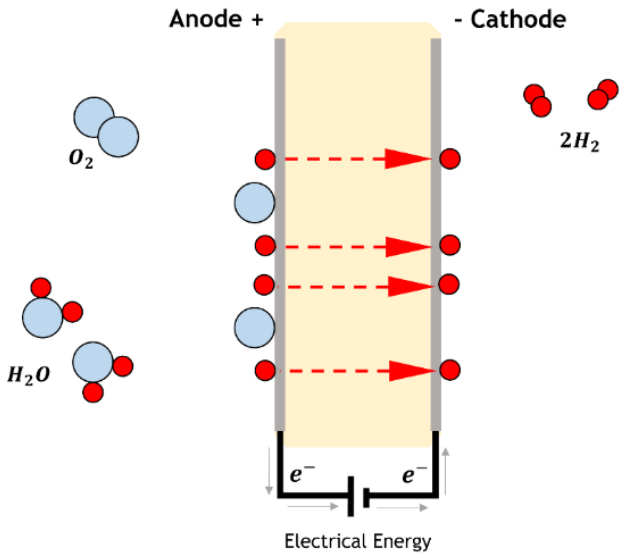

Fig. 3. Single cell electrolyzer of PEM

effects of Galette using the Nernst equation. The Gibbs free energy is defined as [18]:

$$\Delta G = \Delta H - T\Delta S \tag{17}$$

Open circuit voltage for PEM electrolyzer is obtained using Nernst equation:

$$V_0 = 1.229 - 8.5 \times 10^{-3}(T_{PEM} - 298) \tag{18}$$

The single cell voltage of the electrolyzer is defined as follows:

$$V = V_0 + V_{act.a} + V_{act.c} + V_{ohm} \tag{19}$$

Where $V_{act.a}$ indicates the activation voltage drop in the anode, $V_{act.a}$indicates the activation voltage drop in the cathode and indicates theV_{ohm} voltage drop in volts.

Activation voltage drop: The activation voltage drop indicates the electron's readiness for electrochemical reaction. Some of the applied voltage to the electrolyzer is lost due to the transfer of electrons from the surface of the electrodes during the chemical process. The activation energy on both sides of the cathode and anode due to the drop in the activation voltage is modeled by the Volmer-Butler equation as follows:

$$V_{act.i} = \frac{RT}{F}\sinh^{-1}\left(\frac{J}{2J_{0,i}}\right) \tag{20}$$

Where $J_{0.i}$ anode/cathode is current exchange density in amps per square centimeter and is obtained according to the following equation:

$$J_{0,i} = J_i^{ref} \exp\left(-\frac{V_{act.i}}{RT}\right) \tag{21}$$

Ohmic voltage drop: Ohmic voltage drop is the resistance created against the flow of electrons and electrical resistance of the PEM electrolyzer. This voltage drop depends on the type of PEM electrolyzer and the material of the electrodes. The ohmic voltage drop is linearly related to the current density. The ohmic voltage drop caused by the membrane resistance of the electrolyzer is the resistance of the electrolyzer against the transfer of protons and is a function of the membrane thickness (L) in meters, the ion conductivity of the ion exchange membrane (σ_{mem}) in ($1/(\Omega.cm)$) and the current density (J) are defined in terms of amperes per square centimeter as follows [19, 20]:

$$V_{ohm} = JR_{PEM} \tag{22}$$

$$R_{PEM} = \int_0^D \frac{dx}{\sigma_{mem}[\lambda(x)]} \tag{23}$$

$$\lambda(x) = \frac{\lambda_a - \lambda_c}{D}x + \lambda_c \tag{24}$$

Where D is the membrane thickness and $\lambda_a$andλ_c are the water content in anode and cathode, respectively.

$$\sigma_{mem}[\lambda(x)] = [0.5139\lambda(x) - 0.326]\exp[1268(\tfrac{1}{303} - \tfrac{1}{T})] \tag{25}$$

The mass flow of hydrogen produced in the electrolyzer is obtained from the following equation [21]:

$$\dot{N}_{H_2.out} = \frac{J}{2F} = 2\dot{N}_{H_2O.reacted} \tag{26}$$

C. Organic Rankin cycle

The following assumptions are considered for the simulation of the combined power and heating subsystem:

- Thermodynamic balance is established in the system input and output.
- For the subsystem, the assumption of permanent state and permanent flow is established
- The pressure drops in the pipes and the heat drop around in the subsystems are not considered
- The exit state of the condenser is saturated liquid
- Condenser outlet temperature is 15°C higher than ambient temperature
- The evaporator outlet temperature is 15°C lower than the geothermal fluid temperature
- Temperature and pressure are equal at the inlet and outlet of the phase separator
- The temperature at the inlet and outlet of the pressure relief valve is the same
- The pressure at the entrance and exit of the absorber is equal
- The process takes place in the condenser as a constant pressure
- The process takes place in a constant pressure evaporator
- The fluid at the evaporator inlet is in a saturated liquid state
- The processes in the preheaters are done at constant pressure
- The water temperature entering the electrolyzer is the same as the working temperature of electrolyze

Table 1. Mass and energy balance relations in subsystems

Component	Equations	Eq.No
Evaporator	$m_7 = m_8,\ m_1 = m_2,\ m_1(h_1 - h_2) = m_8(h_8 - h_7)$	26
Separator	$m_8 = m_9 + m_{10}$	27
Turbine	$m_9 = m_{11},\ \eta_T = (h_{11} - h_9)/(h_{11.s} - h_9)$	28
Pressure breaker	$m_{10} = m_{12}$	29
Absorber	$m_{11} + m_{12} = m_{13},\ m_{11}h_{11} + m_{12}h_{12} = m_{13}h_{13}$	30
Condenser	$m_{13} = m_5,\ Q_{cond} = m_{13}(h_{13} - h_5)$	31
Pump	$m_5 = m_6\ ,\ \eta_P = (h_5 - h_{6.s})/(h_5 - h_6)$	32
Pre-Heater I	$m_6 = m_7\ ,\ m_2 = m_3\ ,\ m_2(h_2 - h_3) = m_7(h_7 - h_6)$	33
Pre-Heater II	$m_3 = m_4\ ,\ m_14 = m_15\ ,\ m_3(h_3 - h_4) = m_15(h_{15} - h_{14})$	34

Mass balance and energy balance for system subsystems are written according to Table 1 [22]. Finally, the output power of the turbine and the power consumption of the pump are written respectively as follows:

$$W_T = m_9(h_9 - h_{10})$$
$$W_p = m_6(h_6 - h_5) \quad \textbf{(27)}$$

The turbine output power is converted into electric power with a certain efficiency (generator efficiency), which can be written as follows [19]:

$$W_e = W_T \times \eta_G \quad \textbf{(28)}$$

Finally, the total electrical power generated by the system is calculated with the following equation:

$$W_T = W_e - W_p \quad \textbf{(29)}$$

The constants input to the electrolyzer and simulation are shown in Table 2.

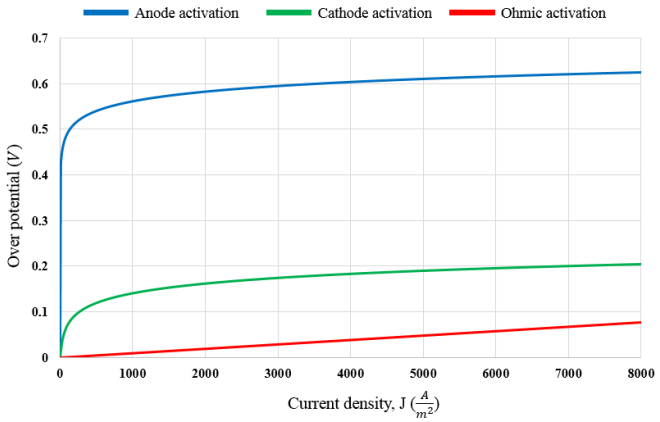

Fig. 4. Changes in cell potential with current density changes

3. RESULTS AND DISCUSSION:

A. Validation:

Figure 4 shows the graph of current density for different voltages. Figure 5 also shows the results obtained in reference [16], comparing the graphs of Figure 4 and Figure 5 shows the accuracy of the results of this work. The results of the simulation indicate a significant rise in cell potential as the current density remains below 300A/m^2. However, once the current density surpasses this threshold, the increase in cell potential becomes marginal. In order to gain a deeper understanding of the electrochemical performance of the PEM electrolyzer, the study examines and presents the ohmic and activation overpotentials separately in Figure 4. The figure illustrates that the ohmic overpotential is negligible and experiences a slight increase with the current density. This observation can be attributed to the high ionic conductivity of the membrane at typical λ values and operating temperatures. Consequently, this results in a lower overall ohmic resistance (RPEM), thereby reducing the ohmic overpotential.

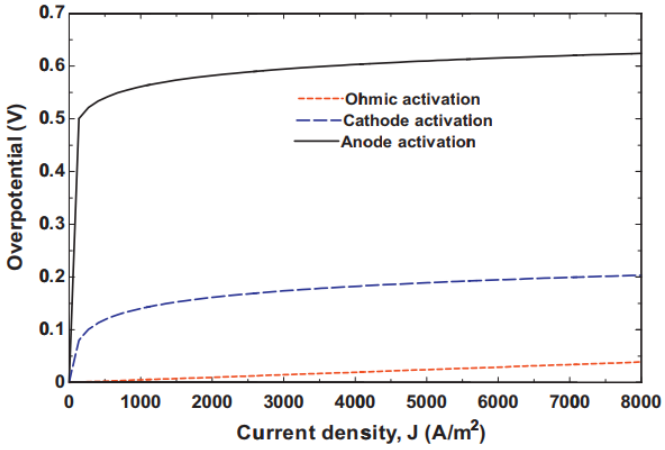

Fig. 5. changes in the cell potential with changes in the reference current density [17]

B. System Output:

Table 3 shows the results of the simulation output for the mentioned fixed inputs (Irradiance = 1000W/m^2, ambient temperature = 25 °C, and wind speed = 2m/s) and for the working

Table 2. Input data

Parameters	Amount	Ref.No
Temperature of the fluid at point 1	140 °C	[23]
Ambient temperature	30 °C	[23]
Condenser Difference Temp.	15 °C	[23]
Evaporator Difference Temp.	15 °C	[23]
Pump Efficiency	75%	[23]
Turbine Efficiency	85%	[23]
Electrolyzer Efficiency	77%	[23]
Electrolyzer Working Point Temp.	70 °C	[23]
Evaporator Pinch Temperature	5 °C	[23]
Generator Efficiency	90%	Selective
Fluid quality at Evaporator Outlet	0.65	Selective
Oxygen Pressure	1.0 atm.	[17]
Hydrogen Pressure	1.0 atm.	[17]
Anode Activation Energy	0.76 kJ/mol.	[17]
Cathode Activation Energy	18 kJ/mol.	[17]
Anode Water Amount	14	[17]
Cathode Water Amount	10	[17]
Membrane Thickness	100 æm	[17]
Anode current density	10000 Amp/m^2	[17]
Cathode current density	10 Amp/m^2	[17]
PV power temperature coefficient (W/K)	0.004	[24]
PV emissivity (-)	0.3	[24]
insulator emissivity (-)	0.3	[24]
optical efficiency of the concentrator (-)	0.85	[24]
PV-absorber thermal resistance (W/m^2)	0.000028	[24]
absorber-insulator thermal resistance (W/m^2)	1	[24]
pinch point temperature difference	10	[24]

Table 3. System Performance

Parameters	Amount	Units
photovoltaic panel Power Generation	1529.4	kW
Turbine Power Generation	1015.3	kW
Pump Power Consumption	126.5	kW
Total Power Generation	2118.2	kW
Hydrogen Generation Rate	0.0060	kg/sec
Energy Efficiency	8.84	%
Exergy Efficiency	36.77	%

fluid butane. According to the table, the amount of power generated by the photovoltaic panel is 1529.4 kW. This amount of production has been obtained according to the panel reference efficiency of 10%, inverter efficiency of 90%, and optical focusing efficiency of 85%. The effect of the nominal efficiency of the panel on the optimal temperature at which the panel can work so that the output power of the whole system is the maximum value, is described in detail in reference [24]. After converting some of the energy received from the sun into electrical energy by the photovoltaic panel, the rest of the energy entered into the cycle, the production power of the turbine is 1015.3 kW. According to the consumption of 126.5 kilowatts of the pump, finally the total electric power produced is 2418.2 kilowatts, and by consuming this amount of energy in the electrolyzer, the amount of hydrogen is produced at 6 grams per second. Total energy efficiency is 8.84% and exergy efficiency is 36.77%.

C. Parametric analysis:

Figure 6 shows the effect of changing the rated efficiency of the photovoltaic panel on the panel's output power. As it is clear from the graph, the changes in nominal efficiency from 8% to 15% increase the output power of the panel from 1223.5 kW to 2294.1 kW. Due to the linear relationship between the panel's output power and its nominal efficiency, which is also affected by the ambient temperature, the output power changes are linear.

Figure 7 shows the effect of ambient temperature change on the photovoltaic panel's output power. As it is clear from the graph, changes in ambient temperature from 0 to 35 15 °C decrease the panel's output power from 1609.9 kW to 1469 kW. It is obvious that the ambient temperature has a negative effect on the functional efficiency of the system, so that with the increase of the ambient temperature, the working efficiency of the panel decreases. With the decrease in working efficiency, the production power of the panel is affected by this increase in temperature, and as a result, the power output of the panel is reduced. The performance of solar cells is adversely affected by higher temperatures due to an increase in internal carrier recombination rates resulting from elevated carrier concentrations. The operating temperature plays a crucial role in the overall photovoltaic conversion process. In certain geographical areas, particularly those characterized by extreme temperature fluctuations, such as desert or tropical regions, the decline in the efficiency of photovoltaic (PV) panels can be particularly notable. To mitigate this issue, it is advisable to opt for PV pan-

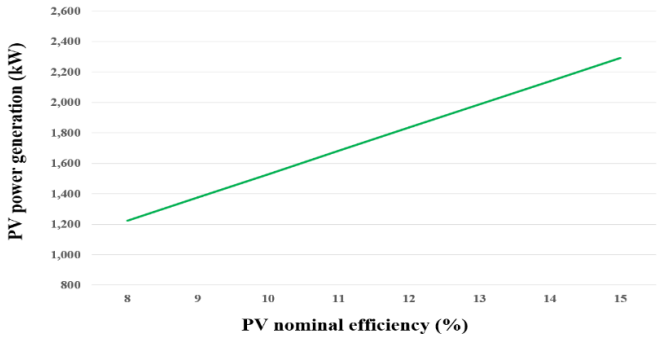

Fig. 6. The effect of changing the nominal efficiency of the photovoltaic panel on its output power

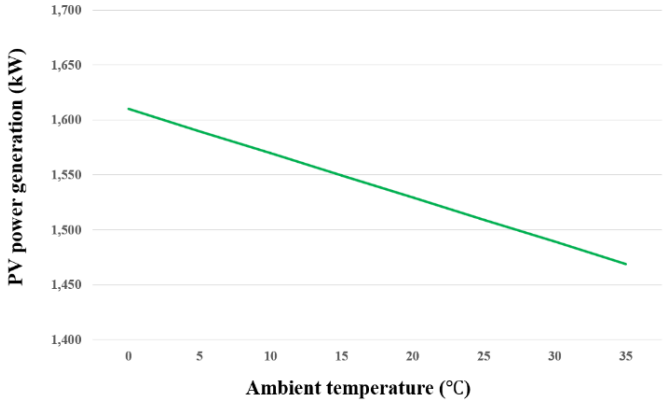

Fig. 7. The effect of ambient temperature changes on photovoltaic panel production power

els that possess a low-temperature coefficient. Figure 8 shows the changes in energy efficiency and exergy of the system with changes in the quality of the fluid at the outlet of the evaporator. As it is clear from the graph, the increase in quality at point 8 increases both efficiencies and the reason for this is the increase in the amount of steam input to the turbine, and as a result, the increase in the production power of the turbine for the fixed input energy of the cycle.

4. CONCLUSIONS

Increasing energy demand, national energy security, and strengthening environmental regulations have increased the need for sustainable and economic energy conversion technologies. As a type of renewable energy, solar energy is the most promising renewable energy source, and photovoltaic cells are the most promising energy conversion technology due to the reduction of investment costs, increased efficiency and low maintenance costs. Therefore, in this paper, a solar system equipped with a concentrator combined with an improved organic Rankine cycle for hydrogen production was evaluated. Concentrated solar energy was considered as the input energy of the system. The total electricity generated by the photovoltaic panel and the organic Rankine cycle is used to produce hydrogen by the electrolyzer. The simulation results showed that the amount of power produced by the photovoltaic panel is 1529.4 kW, the amount of power produced by the turbine is 1015.3 kW, the amount of power consumed by the pump is 126.5 kW, the amount of hydrogen produced is equal to 6 g/s, the energy efficiency is 8.84% and the exergy efficiency is 36.77%. On the other hand, the parametric analysis showed that the increase in nominal efficiency of the panel increases the production power of the photovoltaic panel and the increase in the ambient temperature causes the reduction of the production power of the panel. Also, increasing the quality of the fluid at the outlet of the evaporator increases the energy efficiency and exergy. For future studies, we suggest considering the economic aspects of using the proposed system for hydrogen production purposes, especially on large scales. This will lead to a real insight into producing green hydrogen on an industrial scale.

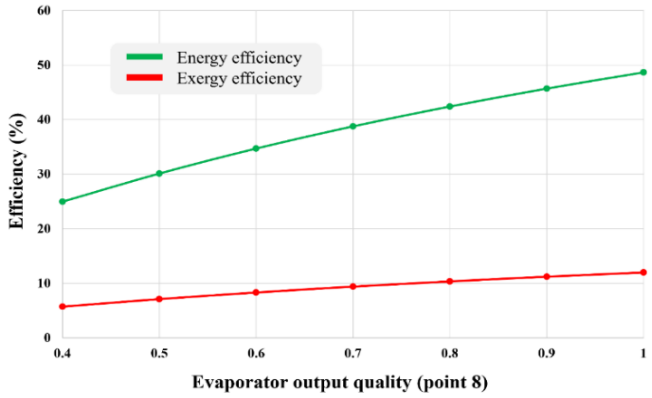

Fig. 8. Changes in energy efficiency and exergy with fluid quality changes at the evaporator outlet

REFERENCES

1. "The future of hydrogen – analysis - iea." https://www.iea.org/reports/the-future-of-hydrogen. Accessed: Jul. 06, 2023.
2. M. Rostami, E. Assareh, R. Moltames, and T. Jafarinejad, "Thermo-economic analysis and multi-objective optimization of a solar dish stirling engine," *Energy Sources, Part A: Recovery, Utilization, and Environmental Effects*, vol. 43, no. 22, pp. 2861–2877, 2021.
3. P. Olivier, C. Bourasseau, and B. Bouamama, "Dynamic and multiphysic pem electrolysis system modelling: A bond graph approach," *International Journal of Hydrogen Energy*, vol. 42, no. 22, pp. 14872–14904, 2017.
4. H. Ganjehsarabi, "Performance assessment of solar-powered high pressure proton exchange membrane electrolyzer: A case study for erzincan," *International Journal of Hydrogen Energy*, vol. 44, no. 20, pp. 9701–9707, 2019.
5. N. Burton, R. Padilla, A. Rose, and H. Habibullah, "Increasing the efficiency of hydrogen production from solar powered water electrolysis," *Renewable and Sustainable Energy Reviews*, vol. 135, p. 110255, 2021.
6. F. M. Nafchi, E. Baniasadi, E. Afshari, and N. Javani, "Performance assessment of a solar hydrogen and electricity production plant using high temperature pem electrolyzer and energy storage," *international journal of hydrogen energy*, vol. 43, no. 11, pp. 5820–5831, 2018.
7. S. M. Alirahmi, E. Assareh, A. Arabkoohsar, H. Yu, S. M. Hosseini, and X. Wang, "Development and multi-criteria optimization of a solar thermal power plant integrated with pem electrolyzer and thermoelectric generator," *International Journal of Hydrogen Energy*, vol. 47, no. 57, pp. 23919–23934, 2022.
8. O. Rejeb, S. M. Alirahmi, E. Assareh, M. E. H. Assad, A. Jemni, M. Bettayeb, and C. Ghenai, "Innovative integrated solar powered polygeneration system for green hydrogen, oxygen, electricity and heat production," *Energy Conversion and Management*, vol. 269, p. 116073, 2022.
9. C. Renno, F. Petito, D. D'Agostino, and F. Minichiello, "Modeling of a cpv/t-orc combined system adopted for an industrial user," *Energies*, vol. 13, no. 13, p. 3476, 2020.

Table 4. Nomenclature

Nomenclature

A_{con}	concentrator area (m^2)	$P_{expander}$	power produced by the expander (W)
A_{pv}	PV panel area (m^2)	P_{pump}	pump consumption (W)
C	concentration ratio	P_{pv}	electric power produced by the PV(W)
C_p	heat capacity(J/kg K)	Q_{conv}	heat convected to the atmosphere (W)
E_{total}	total electric energy produced by the system	Q_{orc}	heat recovered by the ORC (W)
G	direct solar radiation (W/m^2)	Q_{pv}	concentrated radiation on the PV (W)
h	enthalpy (J/kg)	Q_{rad}	heat radiated to the atmosphere (W)
h_{ins}	insulator heat transfer coefficient (W/m^2K)	Q_{Th}	thermal power produced by the CPV (W)
h_{pv}	PV panel heat transfer coefficient (W/m^2K)	R	thermal resistance of each component (W/m^2K)
m	mass of each component (kg)	T_a	ambient temperature (K)
$\dot{m}_{orc}$	ORC fluid mass flow rate (kg/s)	T_{abs}	absorber temperature (K)
$n_{cpv-orc}$	overall efficiency of the system (%)	T_{ins}	insulator temperature (K)
n_{inv}	inverter efficiency (%)	T_{pv}	PV panel temperature (K)
$n_{optical}$	optical efficiency of the concentrator (%)	T_{pv-opt}	optimum temperature of the PV (K)
n_{orc}	ORC system efficiency (%)	T_{ref}	reference temperature (298.16K)
n_{pv}	PV panel efficiency (%)	T_{sky}	sky temperature (K)
n_{pv-ref}	PV nominal efficiency (%)		

10. A. Khouya, "Performance analysis and optimization of a trilateral organic rankine powered by a concentrated photovoltaic thermal system," *Energy*, vol. 247, p. 123439, 2022.
11. A. Khouya, "Performance assessment of a dual loop organic rankine cycle powered by a parabolic trough collector for ammonia and hydrogen production purpose," *International Journal of Ambient Energy*, vol. 43, no. 1, pp. 6149–6166, 2022.
12. C. Golonis, A. Skiadopoulos, D. Manolakos, and G. Kosmadakis, "Assessment of the performance of a low-temperature organic rankine cycle engine coupled with a concentrating pv-thermal system," *Renewable Energy*, vol. 179, pp. 1085–1097, 2021.
13. S. Dubey, J. N. Sarvaiya, and B. Seshadri, "Temperature dependent photovoltaic (pv) efficiency and its effect on pv production in the world–a review," *Energy procedia*, vol. 33, pp. 311–321, 2013.
14. G. Kosmadakis, D. Manolakos, and G. Papadakis, "Simulation and economic analysis of a cpv/thermal system coupled with an organic rankine cycle for increased power generation," *Solar Energy*, vol. 85, no. 2, pp. 308–324, 2011.
15. J. Ji, K. Liu, T.-t. Chow, G. Pei, W. He, and H. He, "Performance analysis of a photovoltaic heat pump," *Applied Energy*, vol. 85, no. 8, pp. 680–693, 2008.
16. A. Kribus, D. Kaftori, G. Mittelman, A. Hirshfeld, Y. Flitsanov, and A. Dayan, "A miniature concentrating photovoltaic and thermal system," *Energy conversion and management*, vol. 47, no. 20, pp. 3582–3590, 2006.
17. P. Ahmadi, I. Dincer, and M. A. Rosen, "Performance assessment and optimization of a novel integrated multigeneration system for residential buildings," *Energy and Buildings*, vol. 67, pp. 568–578, 2013.
18. S. S. Kumar and V. Himabindu, "Hydrogen production by pem water electrolysis–a review," *Materials Science for Energy Technologies*, vol. 2, no. 3, pp. 442–454, 2019.
19. P. Ahmadi, I. Dincer, and M. A. Rosen, "Energy and exergy analyses of hydrogen production via solar-boosted ocean thermal energy conversion and pem electrolysis," *International Journal of Hydrogen Energy*, vol. 38, no. 4, pp. 1795–1805, 2013.
20. E. Aghaie, E. Assareh, H. Yousefi, R. Moltames, A. Fathi, and K. Choubineh, "Exergoeconomic optimization of a novel hydrogen generation system based on geothermal energy," *Environmental Energy and Economic Research*, vol. 5, no. 4, pp. 1–15, 2021.
21. R. Moltames, E. Assareh, F. Mohammadi Bouri, and B. Azizimehr, "Simulation and optimization of a solar based trigeneration system incorporating pem electrolyzer and fuel cell," *Journal of Solar Energy Research*, vol. 6, no. 1, pp. 664–677, 2021.
22. B. Azizimehr, E. Assareh, and R. Moltames, "Thermoeconomic analysis and optimization of a solar micro cchp by using tlbo algorithm for domestic application," *Energy sources, part a: recovery, utilization, and environmental effects*, vol. 42, no. 14, pp. 1747–1761, 2020.
23. H. Ganjehsarabi, "Mixed refrigerant as working fluid in organic rankine cycle for hydrogen production driven by geothermal energy," *International Journal of Hydrogen Energy*, vol. 44, no. 34, pp. 18703–18711, 2019.
24. R. Moltames and R. Roshandel, "Techno-economic analysis of a modified concentrating photovoltaic/organic rankine cycle system," *International Journal of Ambient Energy*, vol. 43, no. 1, pp. 2026–2038, 2022.